IET Renewable Power Generation

Research Article

# Three-phase battery storage system with transformerless cascaded multilevel inverter for distribution grid applications

ISSN 1752-1416
Received on 29th June 2016
Revised 19th November 2016
Accepted on 16th February 2017
E-First on 23rd March 2017
doi: 10.1049/iet-rpg.2016.0629
www.ietdl.org

*Tiago Davi Curi Busarello[1] ✉, Ali Mortezaei[2], Abdullah S. Bubshait[2], Marcelo Godoy Simões[2]*
[1]*Federal University of Santa Catarina, Rua Pomerode 710, Blumenau, Brazil*
[2]*Department of EECS, Colorado School of Mines, 1812 Illinois Street, Golden, USA*
✉ *E-mail: tiago_curi@yahoo.com.br*

**Abstract:** A distributed generator (DG) based on renewable energy is a promising technology for the future of the electrical sector. DGs may benefit utility companies and customers in a variety of perspectives. However, DGs suffer from intermittent behaviour. Storage systems appear as an attractive solution to support the continuous operation of DGs. The technology within the storage also plays an important role, since DGs and storage are connected in medium-voltage grids. The use of batteries and the DC/AC converter in its conventional structure presents drawbacks in such grids. In this context, this study presents a three-phase transformerless battery storage system (BSS) based on a cascaded H-bridge inverter applied to a medium-voltage grid. The BSS is composed of eight equal series connected H-bridge converters, without bulk transformers, for connection to a distribution grid. Each converter contains 75, 12 V/600 Ah lead-acid batteries. The converters are controlled through pulse-width modulation at 600 Hz. The BSS is able to keep working even with a failure of one of its converters. Reactive energy compensation not compensated by an existent passive filter is also performed. A case study with simulated and experimental results obtained through a hardware-in-the-loop system is presented showing the efficacy of the proposed BSS.

## 1 Introduction

It is expected that 80% of the electrical energy supplied in USA in 2050 will be based on renewable sources, as depicted by studies performed by the National Renewable Energy Laboratory (NREL) [1]. Due to the intermittent behaviour of renewable energy sources, such supply can be achieved by the support of energy storage systems. Pumped hydros, compressed air, flywheels, batteries and supercapacitors are examples of technologies for storage systems [2–6]. The choice of the storage technology depends on criteria like cost, life-cycle, energy and power density, and environmental impact [7].

Another criterion is the voltage level of the grid where the storage is connected. A storage system connected to high-voltage grids (approximately hundreds of kilovolts) is mostly based on hydro-pumped or compressed air due to their large power capacity and long life. In low-voltage grids (approximately hundreds of volts), batteries usually are the best choice for storage systems mainly due to their low cost and robustness [8]. In medium-voltage grids (approximately thousands of volts), the storage tends to be made by batteries followed by a DC–AC converter and a bulk 60 Hz-transformer.

Storage applications in medium-voltage grids have been described in the literature [9–12]. In [9], a pumped storage with loss of excitation protection is presented while in [10] a doubly-fed induction-machine-based flywheel energy storage system is introduced. In [11], a battery energy storage system is aggregated to a wind generator (WG) system in order to damp power oscillation produced by the WG system. In [12], a battery storage is connected to the grid through a medium-frequency transformer. All these works show the diversity in storage technology applied in medium-voltage grids.

A common point in these works is the use of a single DC/AC inverter to handle all the power processed from the storage system. Using a single DC/AC converter is unattractive in medium-voltage grids because it requires a series or parallel connection of semiconductors. Moreover, the propagation of high frequencies produced by pulse-width modulation (PWM) into the grid is unavoidable, even when using high-volume filters.

Multilevel inverters seem to be an attractive choice for applications in medium-voltage grids without the necessity of using bulk transformers. Additionally, their semiconductors can be controlled at low frequency, minimising the propagation of high-frequency components. Common topologies of multilevel inverters are diode clamped [13, 14], flying capacitor [15, 16] and cascaded H-bridge (CHB) [17, 18], each one with its feature and validity. The CHB is a potential candidate for BSS applications applied to medium-voltage grids. At the same time, batteries are a prominent technology candidate for storage systems in medium-voltage grids. A study presented recently [7, 19] shows that the reduced relative-energy cost and the possibility of recycling 99% of the battery weight are the main reasons to put them at the top of choice.

Battery storage systems (BSSs) based on multilevel inverters have been reported in the literature [20–25]. In [20, 21], the authors proposed a BSS with six series-connected H-bridge converter. The main purpose is to handle active power equally in the H-bridge converters. In [22], the authors proposed a BSS composed of a modified H-bridge converter. A LC branch is included to produce an auxiliary power loop, which could realise active power exchange between different converters. However, all these works do not mention if the storage system is able to operate under a failure in one of the converters. In [23], the authors proposed a transformerless energy storage system based on a cascade multilevel inverter with star configuration. The system was intended for power levelling of renewable energy sources, as well as for improving power quality and reliability of a power distribution system. Nevertheless, it cannot be concluded how the storage compensates the reactive energy in case there is a passive power filter.

All these works have their efficacy and validity. However, new issues can be addressed. This paper proposes a three-phase transformerless BSS based on a CHB applied to a 4.16 kV grid. The CHB is composed of eight series-connected H-bridge converters. This number of converters allows the CHB to operate without a transformer and to keep the BSS working even when one converter fails. Moreover, the converters use PWM modulation with low switching frequency. The BSS evaluates the state-of-charge (SOC) of each battery bank in order to decide the moments when the batteries should be charged or discharged. The BSS is

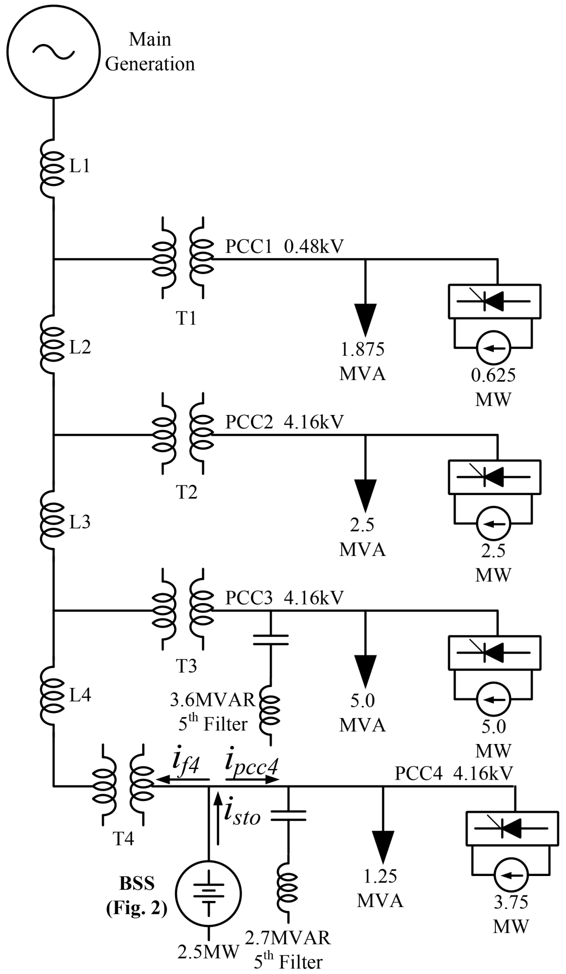


**Fig. 1** *Simplified single-phase diagram of a medium-voltage distribution system with the BSS*

also able to compensate reactive energy at a point of common coupling (PCC) that is not compensated by an already installed passive filter.

Due to the features embedded in the proposed BSS, its configuration is designed for the medium-voltage grids (1–13.8 kV). The installation in other voltage levels is technically unfeasible. In high-voltage grids, as previously stated, the best technology option for a storage system is a pumped-hydro installation. The use of multilevel inverters would require hundreds of series-connected H-bridge converters. On the other hand, in low-voltage grids, the usage of a multilevel inverter is not justified because the available transistors on the market easily handle the voltage value of these grids. Therefore, it is preferable to replace the multilevel inverter with a conventional H-bridge inverter.

## 2 Battery storage system

Fig. 1 presents a simplified single-line diagram of a medium-voltage distribution system with the BSS. The grid is composed of the main generation, distribution transformers, four feeders, linear and non-linear load and passive filters [26]. The BSS is connected to the PCC4.

Fig. 2 presents the single-line diagram of the BSS. The BSS contains eight H-bridge converters. Each converter has a bank of battery with 75 12 V/600 Ah batteries, represented by $V_{dc}$. The output filter is composed only of an inductor. The BSS current and the PCC4 voltage are the variables used in the control strategy. The batteries currents are used to estimate their SOC. A bypass switch is represented at the lower converter in order to emulate a failure.

## 3 Control strategy

Fig. 3 shows the control strategy block diagram. The diagram is for phase $A$, but it is valid also for phases $B$ and $C$. A phase-locked loop is used in order to obtain a synchronised sinusoidal reference related to the PCC4 voltage. The power references for charging ($P_{\text{ref\_charge}}$) and for discharging ($P_{\text{ref\_discharging}}$) are used to charge and discharge the batteries. For the charging process, the power reference is limited to the BSS power rate. For discharging, the BSS can realise this process at its battery capacity rate or the system operator can define the amount of active power to be injected into the grid. The SOC evaluation decides if the BSS is set to charge or discharge the batteries. Information about the PCC4 reactive energy is obtained through the conservative power theory [27, 28] and it is added to the BSS reference if the system operator wants power quality improvement in PCC4. The current control loop block is a closed-loop mesh that controls the BSS output current.

### 3.1 Current control loop

The current control loop guarantees that the BSS output current follows its reference signal independent of its waveform. Fig. 4 presents the current control loop block diagram. The measured current ($I_{\text{sto}}$) is subtracted from the current reference ($I_{\text{sto}*}$) and the resulted error signal ($e$) is sent to the controller, which, in turn, acts on the CHB through the modulated signal ($u$). A voltage feedforward ($v_{\text{PCC4}}$) is added to the current controller output signal. The CHB plus the output filter is represented by a current plant ($G(s)$). The current sensor gain is assumed to be unitary.

The control objective can be expressed in mathematical form as

$$i_{\text{sto}}(t) \to i_{\text{sto}} * (t) \quad \text{as} \quad t \to \infty \tag{1}$$

To guarantee (1), the system must be mathematically modelled. The model can be obtained by a simple application of Kirchhoff's laws at PCC4. This yields the following model that describes the system dynamics

$$L_{\text{sto}} \frac{\mathrm{d}i_{\text{sto}}(t)}{\mathrm{d}t} = v_t(t) - v_{\text{PCC4}}(t) \tag{2}$$

$$L_{\text{sto}} \frac{\mathrm{d}i_{\text{sto}}(t)}{\mathrm{d}t} = \sum_{i=1}^{8} v_{ti} - v_{\text{PCC4}}(t) \tag{3}$$

$$i_{\text{sto}}(t) = i_{f4}(t) + i_{\text{pcc4}}(t) \tag{4}$$

The H-bridge converter terminal voltages can be written as

$$\begin{bmatrix} v_{t1}(t) \\ v_{t2}(t) \\ v_{t3}(t) \\ v_{t4}(t) \\ v_{t5}(t) \\ v_{t6}(t) \\ v_{t7}(t) \\ v_{t8}(t) \end{bmatrix} = \begin{bmatrix} u_1(t)V_{\text{dc}} \\ u_2(t)V_{\text{dc}} \\ u_3(t)V_{\text{dc}} \\ u_4(t)V_{\text{dc}} \\ u_5(t)V_{\text{dc}} \\ u_6(t)V_{\text{dc}} \\ u_7(t)V_{\text{dc}} \\ u_8(t)V_{\text{dc}} \end{bmatrix} \tag{5}$$

where $u1$, $u2$ ,…, $u7$, $u8$ denote the modulation signals for each H-bridge converter. Their signals are continuous and their values are in the range [−1; 1].

To facilitate the controller design and to reduce the model expressions, it is convenient to transform (5) by the definition given in the following equation:

$$\begin{aligned} \lambda(t) &= u_1(t) = u_2(t) = u_3(t) = u_4(t) \\ &= u_5(t) = u_6(t) = u_7(t) = u_8(t) \end{aligned} \tag{6}$$

Therefore, (3) can be rewritten as

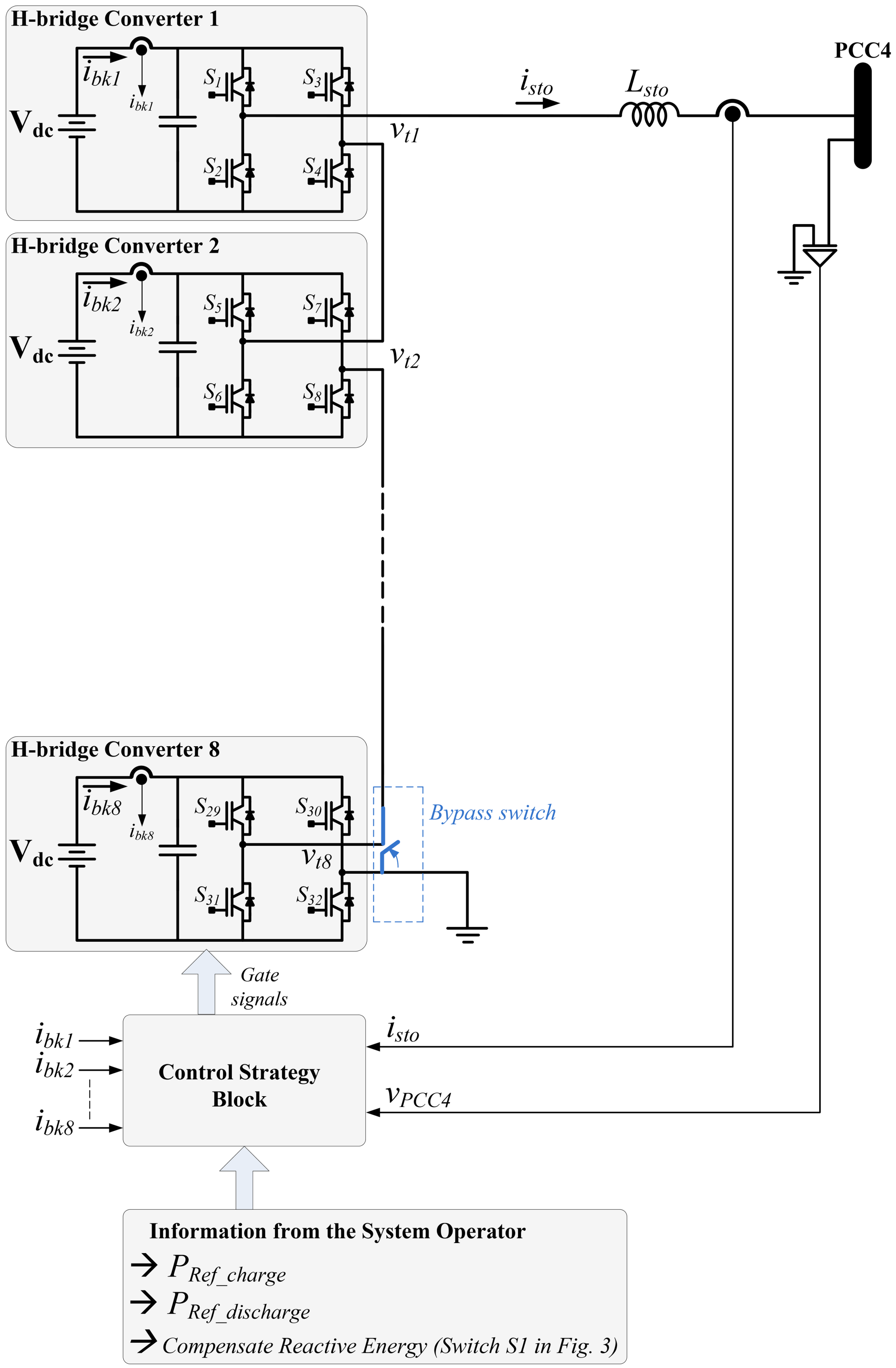


**Fig. 2** *Single-line diagram of the BSS*

$$L_{\text{sto}}\frac{\mathrm{d}i_{\text{sto}}(t)}{\mathrm{d}t} = 8V_{\text{dc}}\lambda(t) - v_{\text{PCC4}}(t) \tag{7}$$

The last term can be considered as disturbance and may be omitted. By applying the perturbation and linearisation technique and taking the Laplace transformation, the CHB plus output filter transfer function ($G$) is given as

$$G(s)\frac{I_{\text{sto}}(s)}{\lambda(s)} = \frac{8V_{\text{dc}}}{sL_{\text{sto}}} \tag{8}$$

The PWM transfer function is given by (9), where $v_{tp}$ is the peak value of the triangular carrier and its value is equal to one

$$\text{PWM}(s) = \frac{1}{v_{tp}} \tag{9}$$

The proportional–integral (PI) controller transfer function is given as

$$C(s) = \frac{\lambda(s)}{e(s)} = \frac{k_p(sT_{\text{PI}} + 1)}{sT_{\text{PI}}} \tag{10}$$

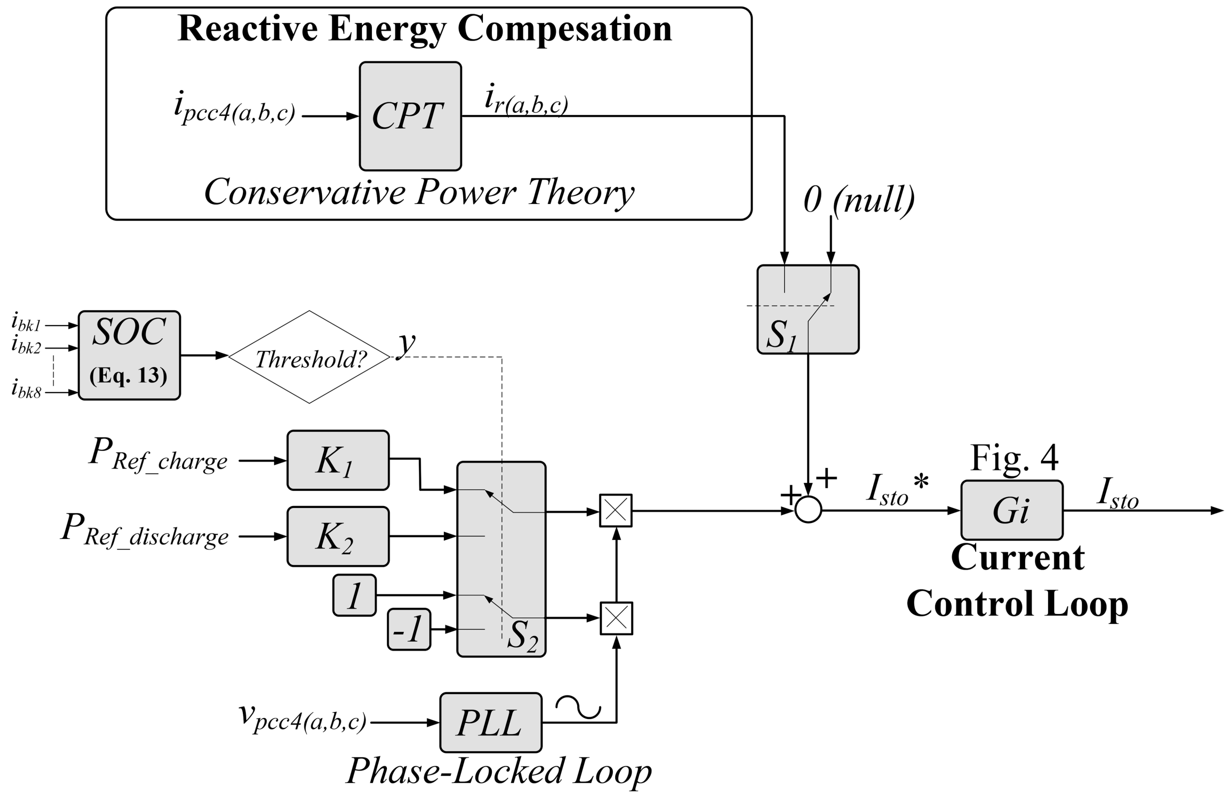


**Fig. 3** *Control strategy block diagram*

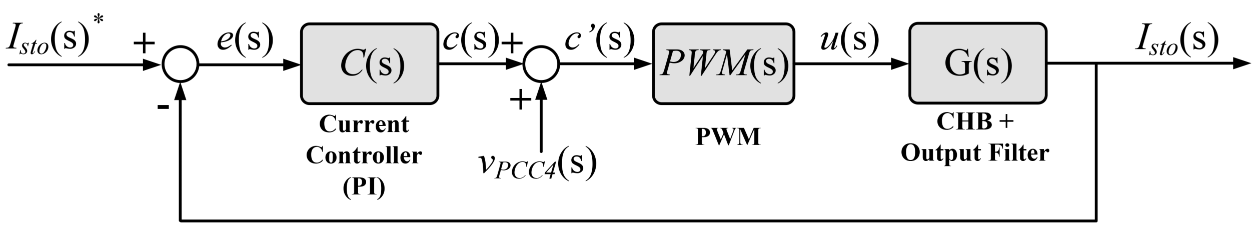


**Fig. 4** *Current control loop block diagram*

The closed-loop transfer function that relates the CHB output current and its reference is given as

$$\frac{I_{\text{sto}}(s)}{I_{\text{sto}}*(s)}=\frac{8V_{\text{dc}}k_p(sT_{\text{PI}}+1)}{s^2T_{\text{PI}}L_{\text{sto}}+s8V_{\text{dc}}k_pT_{\text{PI}}+8V_{\text{dc}}k_p} \tag{11}$$

Omitting the one-sampling delay, the damping factor is given as

$$\xi=\frac{1}{2}\sqrt{\frac{8V_{\text{dc}}k_pT_{\text{PI}}}{L_{\text{sto}}}} \tag{12}$$

$\xi=1$ leads to a critical damping response. Moreover, the time constant $T_{\text{PI}}$ must be assigned to be much longer than the control delay from the viewpoint of control stability.

### *3.2 Operation under failure*

A high number of converters are an advantage due to the possibility of keeping the operation working even under the failure in one or more converters. Each converter must be equipped with a mechanism to bypass its terminals. This mechanism may consist in switching ON the upper transistors of the converter. When a failure happens, the converter under fault is removed through bypassing its terminal points. In this paper, the detection of failure is performed by evaluating the root mean square (RMS) values of the current and voltage at the terminal output of the converter. In case of occurrence of values out of the normal range, a failure is detected. After the failure, the BSS may signalise the system operator or other agent informing them that maintenance is required. The CHB is capable of working with seven modules. No changes are necessary in the control structure. The PCC4 does not notice the failure within the BSS.

## 4 Estimating the SOC and state-of-health (SOH)

Applications covering batteries usually use a model in order to describe their behaviour. The model may contain parameters like SOC, SOH, terminal voltage, cell temperature and internal pressure [29–31]. The battery SOC is not directly measured and an estimation must be done. A simplified way to estimate the SOC is given as [32]

$$\text{SOC}(t)=100\left(\frac{Q_{\text{nom}}-\int_{\tau_0}^{\tau}i_{\text{bat}}(t)\mathrm{d}t}{Q_{\text{nom}}}\right) \tag{13}$$

where $Q_{\text{nom}}$ and $i_{\text{bat}}$ are the battery nominal charge and the instantaneous current, respectively.

In the proposed BSS, the SOC is measured for the average current of all batteries. Moreover, the charge and discharge process are assumed to be the same for all banks. The BSS proposed in this paper considers that the battery is fully charged and discharged when its SOC is 95 and 40%, respectively. These values are used in the SOC inquiry of the control strategy. The choice of these values is based on the spinning reserve criteria [32], which allows the BSS to compensate unpredictable imbalances between the load and generation caused by sudden outages of generating units.

On the other hand, the SOH is a measurement used to qualify the battery condition [7]. The SOH states the age and degradation

**Table 1** System parameters used in the simulation

| Parameter | Value |
|---|---|
| main generation RMS voltage | $V_g = 13.8$ kV |
| PCC4 RMS voltage | $V_{pcc4} = 4.16$ kV |
| system frequency | $f_g = 60$ Hz |
| BSS nominal power | $P_{BSS} = 2.5$ MW |
| $V_{dc}$ voltage for each converter | $V_{dc} = 75 \times 12$ V/600 Ah |
| BSS output inductance | $L_{sto} = 1000$ μH |
| PI time constant | $T_P = 15$ ms |
| sampling frequency | $F_s = 30$ kHz |
| switching frequency for each H-bridge converter | $F_{sw} = 600$ Hz |
| damping factor | $\xi = 1$ |
| PI time constant (adopted) | $T_{PI} = 20$ ms |

**Table 2** THD for phases *A*, *B* and *C* for the simulated results

| THD | Value, % |
|---|---|
| phase *A* | 2.09 |
| phase *B* | 1.94 |
| phase *C* | 2.38 |

of a battery and may be estimated by means of verifying one of the following behaviours: increased float current, increased battery impedance, high cell voltage variation, reduced ability to receive a charge and the counting of the number of cycles. Counting the number of cycles is an attractive manner to evaluate the SOH. A high value is indicative of an old battery. Therefore, each charging cycle is counted and its value is sent to a system operator, which in turn, can use such data to plan the energy delivery and maintenance.

## 5 Case study

The system presented in Fig. 1 was simulated in PSIM software and verified in a real-time control implementation using hardware-in-the-loop (HIL) with the OPAL-RT device. Table 1 presents the parameters used in the simulation and in the HIL system.

Fig. 5 presents the three-phase PCC4 voltage and the BSS current when the BSS is discharging the batteries, i.e. injecting real power into the PCC4. The PCC4 voltage is not purely sinusoidal due to the distribution impedance. The BSS current is sinusoidal and in-phase related to the PCC4 voltage for each phase.

Table 2 presents the total harmonic distortion (THD) of the BSS current for phases *A*, *B* and *C* for the simulated results. Their values are within the limits stated by the IEEE519-2014 standardisation.

Fig. 6 presents the three-phase PCC4 voltage and the BSS current when the BSS is charging the batteries. Similar to the previous case, the BSS current is sinusoidal, but now it is in counter-phase related to the PCC4 voltage, for each phase.

Table 3 presents the THD of the BSS current for phases *A*, *B* and *C* for the simulated results.

Fig. 7 presents the currents for the battery banks of the H-bridge converters 1, 2, 3 and 8. Their waveforms are the same, indicating an equal distribution of power during the charging and discharging process.

Fig. 8 presents the PCC4 voltage and BSS output current for phase *A* during reactive energy compensation. The current is out-of-phase related to the PCC4 voltage, showing the circulation of reactive energy. Similar results are obtained for phases *B* and *C*. The THD of the BSS current for phase *A* is 2.06%.

Fig. 9 presents the PCC4 voltage and the BSS current for phase *A* when one converter is bypassed, exhibiting a failure on it. Initially, the current is sinusoidal and in-phase with the PCC4 voltage. At $t = 0.302$ s, the converter 8 is bypassed. The BSS current is kept unchanged, except for the appearance of a small distortion. This means the BSS does not interrupt its operation when a failure happens in one of its converters. The THD of the BSS current for phase *A* after the failure is 4.74%.

Fig. 10 presents the CHB terminal voltage when the converter is bypassed. The terminal voltage is composed of 15 levels before and after the failure. Afterwards, the terminal voltage presents minimal distortions. The voltage THD in the simulated result is 9.84%. Note that this voltage is before filtering.

## 6 Discussion

Distributed generators (DGs) bring potential benefits to utility companies and customers. Utilities can benefit by increasing the host capacity, reducing the power transmission and distribution losses, regulating the voltage profile at PCCs, and compensating the power factor. Customers can receive uninterrupted electrical energy even with malfunction in the distribution system. Moreover, if customers are the owner of a DG, they can have their energy bill reduced and earn credits if they sell their excess energy.

Renewable energy sources are usually the primary source of DGs. As a result, the power dispatch of DGs is dependent on the intermittent nature of such sources. For example, wind-based DG supplies active power according to the wind speed, which can vary in several timescales, from seconds to hours. Therefore, the intermittent behaviour of DGs can deplete their benefits in the electrical sector.

Even though fuel cells and batteries are non-renewable energy sources, they also can be used as primary sources in DGs. The biggest advantage in this case is the controllable power dispatch.

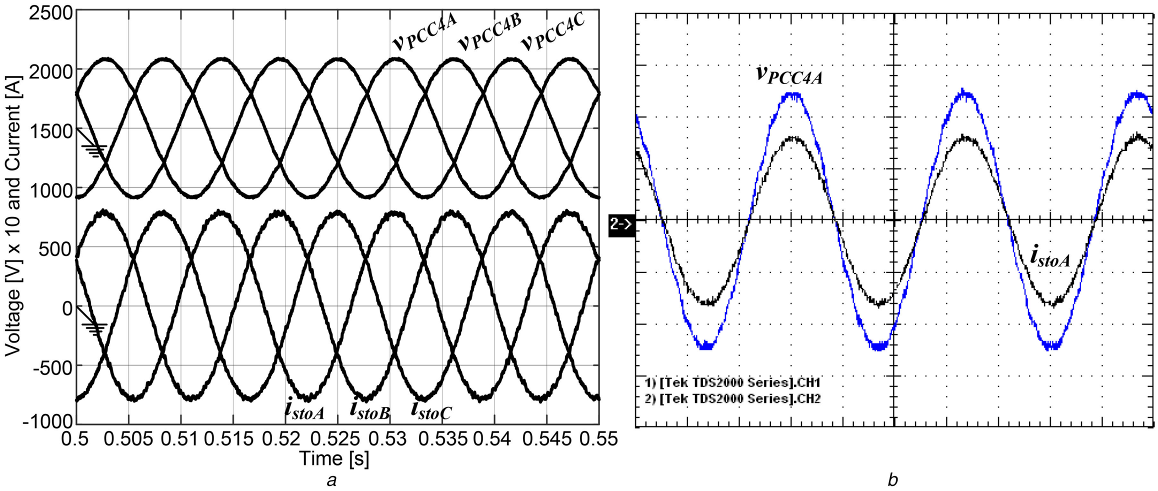


**Fig. 5** *PCC4 voltage and the BSS current when the BSS is discharging the batteries*
***(a)*** Simulated results for the three phases, ***(b)*** Experimental results for phase *A* (Ch1: 2400 V/div; Ch2: 500 A/div)

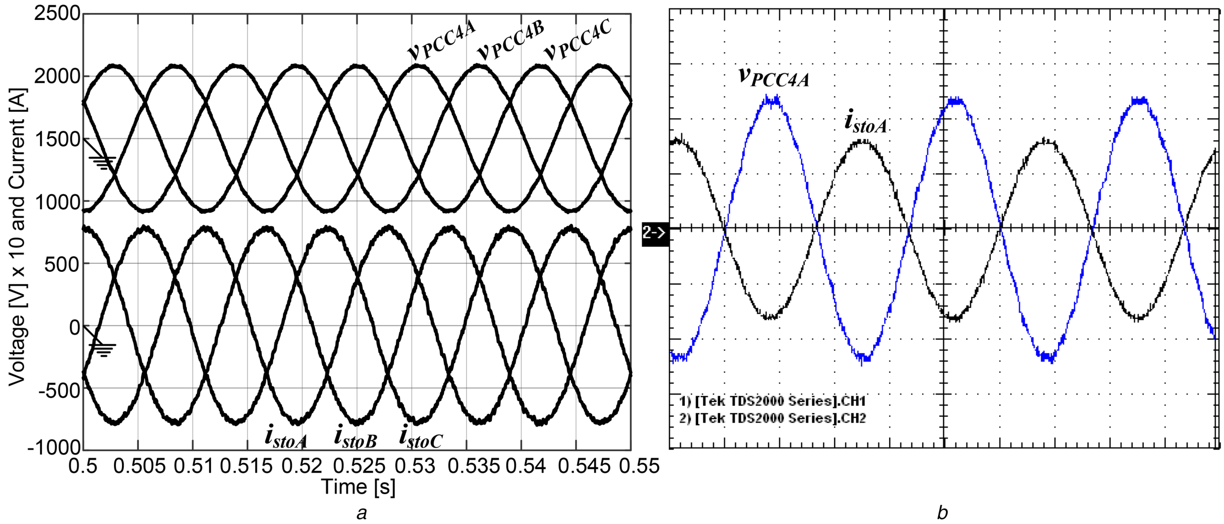


**Fig. 6** *PCC4 voltage and the BSS current when the BSS is charging the batteries*
***(a)*** Simulated results for the three phases, ***(b)*** Experimental results for phase *A* (Ch1: 2400 V/div; Ch2: 500 A/div)

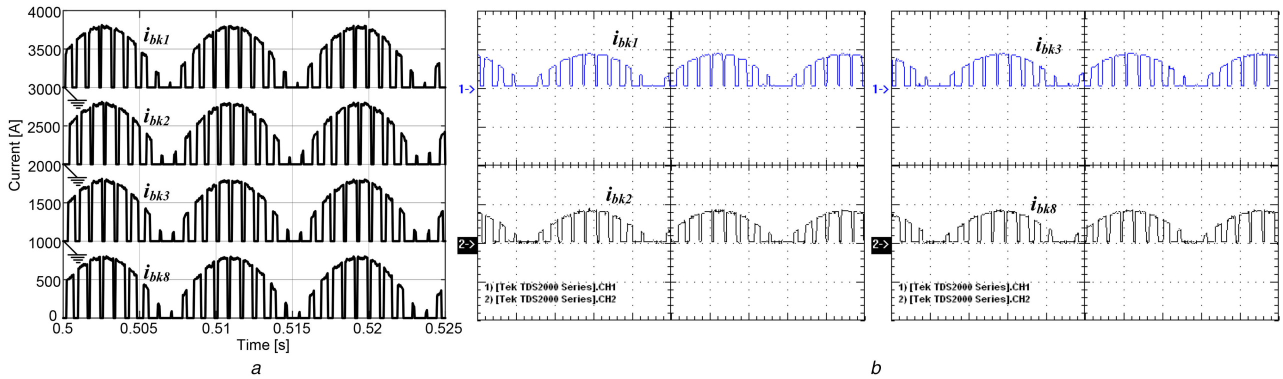


**Fig. 7** *Currents for the battery banks of the H-bridge converters 1, 2, 3 and 8*
***(a)*** Simulated results, ***(b)*** Experimental results (Ch1, Ch2: 750 A/div)

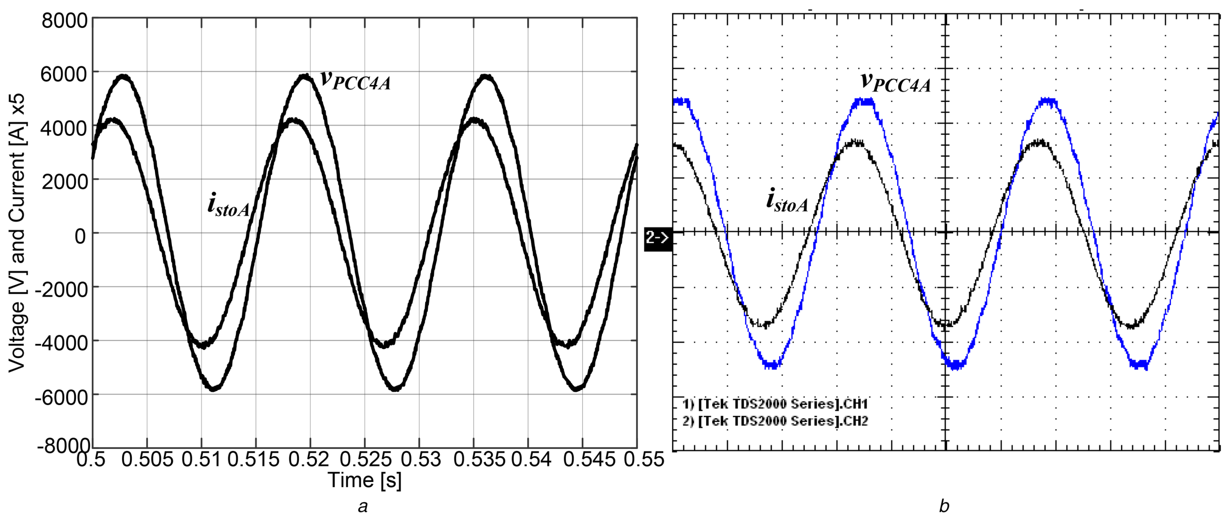


**Fig. 8** *PCC4 voltage and BSS output current for phase A during reactive energy compensation*
***(a)*** Simulated results, ***(b)*** Experimental results (Ch1: 2400 V/div; Ch2: 500 A/div)

**Table 3** THD of the BSS current for phases A, B and C for the simulated results

| THD | Value, % |
|---|---|
| phase *A* | 2.14 |
| phase *B* | 2.13 |
| phase *C* | 2.10 |

Active power is supplied in required times according to the desired criteria.

The BSS proposed in this paper is a DG for the distribution system presented in Fig. 1. Therefore, the BSS supports a proper operation of the distribution system. The system operator can plan the power dispatch considering the BSS. In this context, an internal failure in any DG followed by its full interruption is not desired for the system operator. The proposed BSS has the ability to keep operating under a failure, contributing to the reliability of the distribution system.

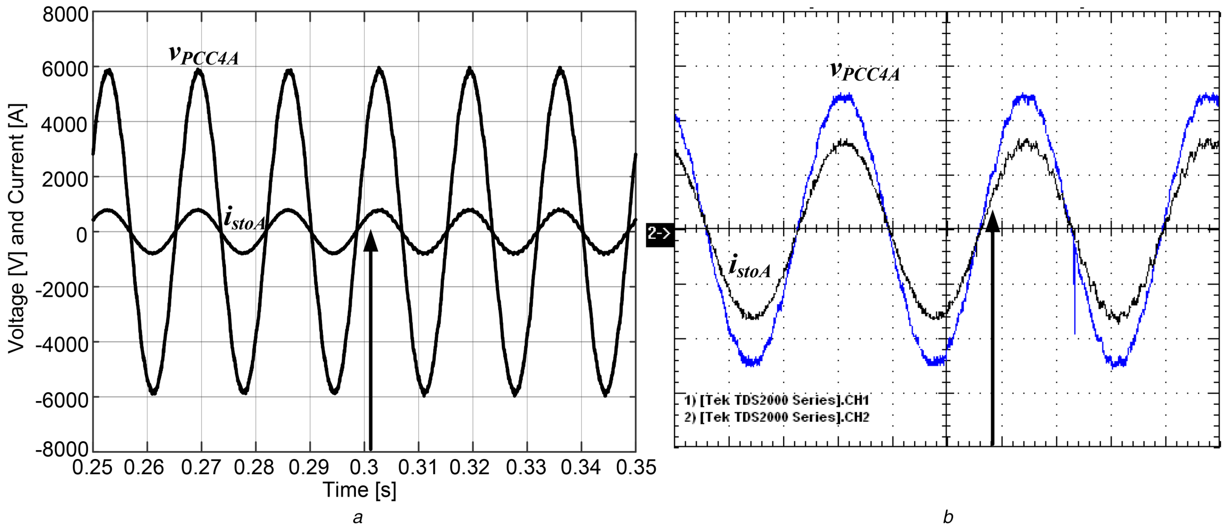


**Fig. 9** *PCC4 voltage and the BSS current for phase A when one converter is bypassed*
***(a)*** Simulated results, ***(b)*** Experimental results (Ch1: 2400 V/div; Ch2: 500 A/div)

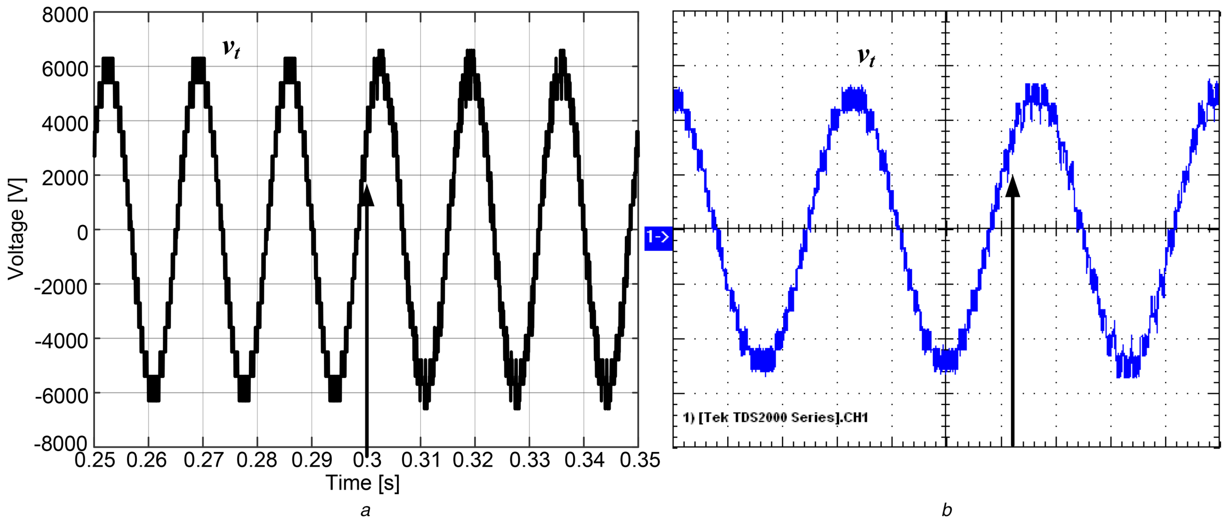


**Fig. 10** *CHB terminal voltage when the converter is bypassed*
***(a)*** Simulated results, ***(b)*** Experimental results (Ch1: 2400 V/div)

The injected active power into the distribution system by the BSS may be used to regulate the voltage profile, to regulate the fundamental frequency and to reduce the distribution power losses. This is an interesting action because the PCC4 is far from the main generation and usually receives a deteriorated voltage. Even though these issues are not the objective of this paper, they can be implemented without changing the physical structure. The installation of the BSS at PCC4 also makes the loads on this PCC receive electrical energy from a closer source, reducing the distribution power losses. This facilitates a system operator in managing the distribution system. Similar analysis can be performed by reactive energy. The proposed BSS is designed to compensate only the reactive energy which is not being compensated by a tuned passive filter due to detuning. Moreover, reactive energy may be delivered or consumed by the BSS in order to regulate the voltage profile at PCCs or to compensate the power factor.

The cost of an application depends on a variety of factors. It is not trivial and is difficult to determine how costly the implementation of a solution is. The proposed BSS is constructed with eight equal series-connected H-bridge converters, each one with a battery bank composed of 75 batteries. At first glance, the BSS seems a high cost solution due to the amount of components employed. However, this opinion is extinguished when maintenance is taken into account. Once the structure of the BSS is modular, the exchange of a damaged converter to a new one is as easy a task as a drawer exchange in a rack. There is no need to turn off the BSS to exchange the converters, assured by a bypass switch. Therefore, in this case the BSS does not account for the cost of interruption.

## 7 Conclusions

This paper presents a three-phase BSS with a transformerless-cascaded multilevel inverter for distribution grid applications. The BSS is composed of eight series-connected H-bridge converters, making it unnecessary to use any bulk transformer. Each converter contains a battery bank made up of 75 12 V/600Ah lead-acid batteries. The BSS is also able to keep working even if one of its converters fails. Moreover, reactive energy compensation is also performed by the proposed BSS.

A case study with simulated and experimental results in HIL system shows the performance of the BSS to be excellent. The charging and discharging processes result in sinusoidal currents that are in-phase with the voltages at the point of common coupling, PCC4. In both cases, the power distribution among the converter is always linear, showing an equal-power processing. A failure in one of the H-bridge converters is emulated and the results demonstrate that the BSS kept working uninterrupted. Therefore, the proposed BSS is an attractive solution for applications in medium-voltage grids, contributing to the reliability and to the uninterrupted supply of the distribution system. Moreover, new functions can be embedded in the proposed BSS without the necessity of changing the physical structure. This increases the options of management of the system operator. The simulation used in this paper will be freely available on the author's webpage: https://sites.google.com/site/busarellosmartgrid/home.

## 8 References


[1] Shahan, Z.: '*80% clean, renewable energy by 2050: more than possible, but need more political will*' (Scientific American., 2012)

[2] Nguyen, T.D., Tseng, K.J., Zhang, S., *et al.*: 'A novel axial flux permanent-magnet machine for flywheel energy storage system: design and analysis', *IEEE Trans. Ind. Electron.*, 2011, **58**, (9), pp. 3784–3794

[3] Deane, J.P., McKeogh, E.J., Gallachoir, B.P.O.: 'Derivation of intertemporal targets for large pumped hydro energy storage with stochastic optimization', *IEEE Trans. Power Syst.*, 2013, **28**, (3), pp. 2147–2155

[4] Le, H.T., Santoso, S.: 'Operating compressed-air energy storage as dynamic reactive compensator for stabilising wind farms under grid fault conditions', *IET Renew. Power Gener.*, 2013, **7**, (6), pp. 717–726

[5] Ristic, M., Gryska, Y., McGinley, J.V.M., *et al.*: 'Supercapacitor energy storage for magnetic resonance imaging systems', *IEEE Trans. Ind. Electron.*, 2014, **61**, (8), pp. 4255–4264

[6] Pickard, W.F.: 'The history, present state, and future prospects of underground pumped hydro for massive energy storage', *Proc. IEEE*, 2012, **100**, (2), pp. 473–483

[7] Du, P., Lu, N.: '*Energy storage for smart grids: planning and operation for renewable and variable energy resources (VERs)*' (Academic Press, 2014)

[8] Cresta, M., Gatta, F.M., Geri, A., *et al.*: 'Optimal operation of a low-voltage distribution network with renewable distributed generation by NaS battery and demand response strategy: a case study in a trial site', *IET Renew. Power Gener.*, 2015, **9**, (6), pp. 549–556

[9] Li, B., Duan, Z., Wang, X., *et al.*: 'Loss-of-excitation analysis and protection for pumped-storage machines during starting', *IET Renew. Power Gener.*, 2016, **10**, (1), pp. 71–78

[10] Abdel-Khalik, A.S., Elserougi, A.A., Massoud, A.M., *et al.*: 'Fault current contribution of medium voltage inverter and doubly-fed induction-machine-based flywheel energy storage system', *IEEE Trans. Sustain. Energy*, 2013, **4**, (1), pp. 58–67

[11] Xu, G., Xu, L., Morrow, J.: 'Power oscillation damping using wind turbines with energy storage systems', *IET Renew. Power Gener.*, 2013, **7**, (5), pp. 449–457

[12] Krishnamoorthy, H.S., Rana, D., Garg, P., *et al.*: 'Wind turbine generator–battery energy storage utility interface converter topology with medium-frequency transformer link', *IEEE Trans. Power Electron.*, 2014, **29**, (8), pp. 4146–4155

[13] Bloh, J.V., Doncker, R.W.D.: 'Design rules for diode-clamped multilevel inverters used in medium-voltage applications'. VIII IEEE Int. Power Electronics Congress, 2002. Technical Proc. CIEP 2002, 2002, pp. 165–170

[14] Akagi, H., Hatada, T.: 'Voltage balancing control for a three-level diode-clamped converter in a medium-voltage transformerless hybrid active filter', *IEEE Trans. Power Electron.*, 2009, **24**, (3), pp. 571–579

[15] Tian, K., Wu, B., Narimani, M., *et al.*: 'A capacitor voltage-balancing method for nested neutral point clamped (NNPC) inverter', *IEEE Trans. Power Electron.*, 2016, **31**, (3), pp. 2575–2583

[16] Janik, D., Kosan, T., Blahnik, V., *et al.*: 'Complete solution of 4-level flying capacitor converter for medium-voltage drives with active voltage balancing control with phase-disposition PWM'. 16th European Conf. on Power Electronics and Applications (EPE'14-ECCE Europe), 2014, 2014, pp. 1–8

[17] Abolhassani, M.: 'Modular multipulse rectifier transformers in symmetrical cascaded H-bridge medium voltage drives', *IEEE Trans. Power Electron.*, 2012, **27**, (2), pp. 698–705

[18] Liang, X., He, J.: 'Load model for medium voltage cascaded H-bridge multi-level inverter drive systems', *IEEE Power Energy Technol. Syst. J.*, 2016, **3**, (1), pp. 13–23

[19] Mateo, C., Reneses, J., Rodriguez-Calvo, A., *et al.*: 'Cost–benefit analysis of battery storage in medium-voltage distribution networks', *Transm. Distrib. IET Gener.*, 2016, **10**, (3), pp. 815–821

[20] Kawakami, N., Ota, S., Kon, H., *et al.*: 'Development of a 500-kW modular multilevel cascade converter for battery energy storage systems', *IEEE Trans. Ind. Appl.*, 2014, **50**, (6), pp. 3902–3910

[21] Vasiladiotis, M., Rufer, A.: 'Balancing control actions for cascaded H-bridge converters with integrated battery energy storage'. 15th European Conf. on Power Electronics and Applications (EPE), 2013, 2013, pp. 1–10

[22] Jiang, W., Huang, L., Zhang, L., *et al.*: 'Control of active power exchange with auxiliary power loop in single-phase cascaded multilevel converter based energy storage system', *IEEE Trans. Power Electron.*, 2016, **PP**, (99), pp. 1–1

[23] Maharjan, L., Inoue, S., Akagi, H.: 'A transformerless energy storage system based on a cascade multilevel PWM converter with star configuration', *IEEE Trans. Ind. Appl.*, 2008, **44**, (5), pp. 1621–1630

[24] Vasiladiotis, M., Rufer, A.: 'Analysis and control of modular multilevel converters with integrated battery energy storage', *IEEE Trans. Power Electron.*, 2015, **30**, (1), pp. 163–175

[25] Simões, M.G., Busarello, T.D.C., Bubshait, A.S., *et al.*: 'Interactive smart battery storage for a PV and wind hybrid energy management control based on conservative power theory', *Int. J. Control*, 2016, **89**, (4), pp. 850–870

[26] 'IEEE recommended practices and requirements for harmonic control in electrical power systems', IEEE Std 519-1992, 1993, pp. 1–112

[27] Tenti, P., Paredes, H.K.M., Mattavelli, P.: 'Conservative power theory, a framework to approach control and accountability issues in smart microgrids', *IEEE Trans. Power Electron.*, 2011, **26**, (3), pp. 664–673

[28] Busarello, T.D.C., Pomilio, J.A.: 'Bidirectional multilevel shunt compensator with simultaneous functionalities based on the conservative power theory for battery-based storages', *Transm. Distrib. IET Gener.*, 2015, **9**, (12), pp. 1361–1368

[29] Pavlov, D.: '*Lead-acid batteries: science and technology*' (Elsevier, 2015)

[30] Achaibou, N., Haddadi, M., Malek, A.: 'Modeling of lead acid batteries in PV systems', *Energy Procedia*, 2012, **18**, pp. 538–544

[31] Salameh, Z.M., Casacca, M.A., Lynch, W.A.: 'A mathematical model for lead-acid batteries', *IEEE Trans. Energy Convers.*, 1992, **7**, (1), pp. 93–98

[32] Chakraborty, S., Simoes, M.G., Kramer, W.E.: '*Power electronics for renewable and distributed energy systems: a sourcebook of topologies, control and integration*' (Springer Science & Business Media, 2013)